Monitoring Active Patient Participation During Robotic Rehabilitation: Comparison Between a Robot-Based Metric and an EMG-Based Metric

Elisabeth R. Jensen, Kim K. Peper, *Graduate Student Member, IEEE*, Marion Egger, Friedemann Müller, Erfan Shahriari, and Sami Haddadin, *Senior Member, IEEE*

***Abstract*— While rehabilitation robots present a much-needed solution to improving early mobilization therapy in demanding clinical settings, they also present new challenges and opportunities in patient monitoring. Aside from the fundamental challenge of quantifying a patient's voluntary contribution during robot-led therapy motion, many sensors cannot be used in clinical settings due to time and space limitations. In this paper, we present and compare two metrics for monitoring a patient's active participation in the motion. The two metrics, each derived from first principles, have the same biomechanical interpretability, i.e., active work by the patient during the robotic mobilization therapy, but are calculated in two different spaces (Cartesian vs. muscle space). Furthermore, the sensors used to quantify these two metrics are fully independent from each other and the associated measurements are unrelated. Specifically, the *robot-based work* metric utilizes robot-integrated force sensors, while the *EMG-based work* metric requires electrophysiological sensors. We then apply the two metrics to therapy performed using a clinically certified, commercially available robotic system and compare them against the specific instructions given to the healthy subjects as well as against each other. Both metric outputs qualitatively match the expected behavior of the healthy subjects. Additionally, strong correlations (median $R^2 > 0.80$) are shown between the two metrics, not only for healthy subjects ($n = 12$) but also for patients ($n = 2$), providing solid evidence for their validity and translatability. Importantly, the *robot-based work* metric does not rely on any sensors outside of those integrated into the robot, thus making it ideal for application in clinical settings.**

***Index Terms*— Assist as needed, intensive care unit, participation assessment, rehabilitation robotics.**

Manuscript received 6 July 2023; revised 19 September 2023; accepted 4 October 2023. Date of publication 16 October 2023; date of current version 26 October 2023. This work was supported in part by the Federal Ministry of Education and Research of the Federal Republic of Germany (BMBF) as part of the project Mobilisation Intensiv-Pflegebedürftiger durch adaptive Robotik (MobIPaR) under Grant 16SV7987; in part by the project Artificial Intelligence for Neuro Deficits (AI.D) under Grant 16ME0539K; and in part by the Bavarian Ministry of Economic Affairs, Regional Development and Energy (StMWi Bayern) as part of the Lighthouse Initiative Geriatronics Project X under Grant IUK-1807-0007// IUK582/001. *(Corresponding author: Elisabeth R. Jensen.)*

This work involved human subjects or animals in its research. Approval of all ethical and experimental procedures and protocols was granted by the Ethics Committee of the Technical University of Munich under Application No. 2022-623-S-KH and the Ludwig Maximilians University of Munich ethics committee under Application No. 18-645.

Elisabeth R. Jensen, Kim K. Peper, and Sami Haddadin are with the School of Computation, Information and Technology, Department of Computer Engineering, Munich Institute of Robotics and Machine Intelligence (MIRMI), Technical University of Munich, 80333 Munich, Germany (e-mail: elisabeth.jensen@tum.de).

Marion Egger and Friedemann Müller are with Schön Klinik Bad Aibling Harthausen, 83043 Bad Aibling, Germany.

Erfan Shahriari is with the School of Computation, Information and Technology, Department of Computer Engineering, Munich Institute of Robotics and Machine Intelligence (MIRMI), Technical University of Munich, 80333 Munich, Germany, and also with the Department of Mechanical Engineering, Massachusetts Institute of Technology, Cambridge, MA 02139 USA.

Digital Object Identifier 10.1109/TNSRE.2023.3323390

I. Introduction

THE main priority of intensive care facilities is to treat life-threatening ailments, which requires a major emphasis on bed rest and immobilization. Unfortunately, bed rest and immobilization are associated with secondary complications of the musculoskeletal and cardiovascular systems [1], [2], [3], from which recovery is generally slow and which can eventually overshadow the initial ailment [4]. For example, the development of intensive care unit-acquired weakness (ICU-AW), which can be attributed to a combination of neural and muscular dysfunction, has been observed in up to 67% of patients admitted to the ICU and is associated with poor clinical outcomes [5], [6], [7]. Impaired skeletal muscle function has been observed upwards of five years after hospital release [8], [9]. Early mobilization has long been suggested as a way to improve the recovery of critical care patients [10] and the benefits have been demonstrated in a number of randomized controlled trials [11]. Importantly, early mobilization has recently been incorporated into the established norms and standards for care of ICU patients with pulmonary disfunction in Germany [12].

Robotic devices are gaining increasing traction as assistive tools for various aspects of healthcare. They have been especially well-received in the area of neuromotor rehabilitation, because they enable more extended and consistent patient training with minimal physical effort by the therapists, simultaneous treatment of multiple patients, and the ability to

monitor progress [13], [14]. Robot-based mobilization also has enormous potential in the critical care setting [15], [16]. For instance, robotic systems may be used to reduce the physical burden as well as the safety risks associated with mobilizing frail, physiologically unstable and/or agitated patients [17], [18], [19]. Further, the barrier of personnel limitations, such as insufficient staff numbers with adequate training level and insufficient funding, which often limits the implementation of early mobilization, may be mitigated through the use of robotic systems [17], [19].

Robots have also opened the door for new rehabilitation strategies and approaches through the use of intelligent control algorithms. It is well known that voluntary drive and energy expenditure, i.e., active patient participation, are critical to preventing muscle strength loss and promoting recovery during early mobilization [20]. Furthermore, voluntary drive is key for motor learning [21]. To address this, robot control strategies have been developed to intelligently adapt the support level to the needs of the patient ("assist-as-needed", AAN), e.g. using machine learning approaches [22], [23], [24]. For example, an energy-based AAN control algorithm was recently integrated into a commercial robotic system, designed for use in the ICU, and an initial clinical study reported positive results [16], [25]. This AAN control algorithm is designed to empower patients and promote active participation by supplementing the energy that the patient is not capable of generating him- or herself. Detailed results of this clinical study have not yet been reported.

Given the separation between patient and therapist and the importance of voluntary drive during robotic rehabilitation, it is important to continuously monitor the patient's level of self-initiated movement [26]. This is particularly important due to the so-called "slacking hypothesis", which is based on observations that patients tend to reduce their effort and let the robot drive the motion if too much support is offered [27]. This, in turn, may negatively impact rehabilitation outcomes, following the evidence described above.

Neural drive in the motor cortex is the origin of movement and can, in theory, be assessed using electroencephalography (EEG). At least one research group has shown that EEG can be used to differentiate between active and passive walking with a robotic device [28]. Electromyography (EMG) provides a more movement-specific measure of neuromotor activity, i.e., muscle activity modulation, and is widely used in the laboratory setting [29].

Unfortunately, electrophysiological sensors are impractical for regular use in ICU settings [30]. Therefore, it is also important to find methods for estimating the patient's active movement generation, which involve only sensors that can be integrated into the robotic system, e.g., interaction force, motor torque, and robot link angle (velocity) sensors. However, estimating active participation can be challenging when only force or motion sensing is used, especially when the robot's support changes. For example, when the support is low, the magnitude of the interaction force - and thus its variation - may decrease, making it more difficult to assess the patient's behavior based solely on the force/torque changes [26]. A similar phenomenon occurs when the support is high, and the observation metric relies solely on the motion.

A. Related Works

As introduced above, EMG measurements have been used by a number of research groups to estimate joint torques, also in the context of robotic support with AAN control algorithms [31], [32]. For example, by using EMG measurement data as an input for computational models of the musculoskeletal system, the actual joint torque may be estimated, which may then be used to derive the deficient joint torque [33]. Additionally, a number of biomechanical measures have been explored for quantifying patient performance, both in terms of quality and quantity. These techniques use force and torque signals to quantify the amount of robotic assistance provided to the patient and have the advantage that the integrated sensors of the robot suffice and no additional equipment, such as EMG or motion capture, is needed [34]. Such measures include: the (arbitarily) weighted sum of human-robot interaction torques [26], the human active torque, estimated by subtracting a passive baseline [35], musculoskeletal modeling-based operator strength estimation [36], total work performed by the robot [37], "useful force", i.e., the force applied along the target direction, as well as task-specific kinematic and dynamic performance indicators [38]. While some of the listed metrics are either biomechanically interpretable or practicable for use in a clinical setting, none combine both of these important features. An exception to this is the integrated power metric presented in [39], which is both interpretable and practicable. However, to the knowledge of the authors, neither this nor other metrics have been effectively verified or validated in human subject experiments.

B. Contribution Statement

In this work, we derive and compare two metrics for quantifying a patient's active participation during robot-led lower limb mobilization. The two metrics are chosen for their identical biomechanical interpretability, i.e., the work actively contributed by the patient to the mobilization therapy, and their non-overlapping sensor requirements. The first metric only requires the robot's integrated sensors, making it highly practical for clinical application, while the second requires only electromyography (EMG) sensors as well as a basic measurement of the patient kinematics. Both metrics are derived using first order principles (preferentially) and well-established correlation factors (only where necessary). We evaluate and compare these metrics using a commercially available robotic rehabilitation system and healthy subjects as well as patients. Both full support and AAN support are considered in order to test whether the predictive capacity is affected by the variable robot support level. We then provide initial evidence that patients may participate more actively when receiving AAN-based therapy as opposed to full support therapy in the ICU.

II. Theory

Here, we derive two metrics for quantifying the human's active contribution during a cyclic robot-aided movement

rehabilitation task. This may be referred to as the "productive work" performed by the human, i.e., the work contributed toward the specified task. The first metric is based on conservation of energy and uses force sensors integrated in the robot. The second metric considers electrophysiological sensor-based estimation of muscle forces. These metrics quantify the same physical phenomenon, but are based on fully independent measurements; therefore, each serves as a means of verifying the other. In the following subsections, we begin by presenting the dynamics of the musculoskeletal system before deriving first the *robot-based work* and then the *EMG-based work* metrics.

A. Musculoskeletal Dynamics

Human limb movement is controlled by muscle activation. Considering $\boldsymbol{\tau}_h \in \mathbb{R}^n$ as the joint torque of the n-degrees-of-freedom human limb associated with muscle activation, the limb's motion can be described with the following dynamics equation:

$$\begin{aligned}\boldsymbol{M}_h(\boldsymbol{q}_h)\ddot{\boldsymbol{q}}_h + \boldsymbol{C}_h(\boldsymbol{q}_h, \dot{\boldsymbol{q}}_h)\dot{\boldsymbol{q}}_h + \boldsymbol{g}_h(\boldsymbol{q}_h) \\ + \boldsymbol{d}_h(\dot{\boldsymbol{q}}_h) + \boldsymbol{k}_h(\boldsymbol{q}_h) = \boldsymbol{\tau}_h.\end{aligned} \tag{1}$$

Here, $\boldsymbol{q}_h \in \mathbb{R}^n$ represent the limb's joint angles, $\boldsymbol{M}(\boldsymbol{q}_h)$, $\boldsymbol{C}_h(\boldsymbol{q}_h, \dot{\boldsymbol{q}}_h) \in \mathbb{R}^{n\times n}$ are the inertia and the centrifugal and Coriolis matrices, respectively, and $\boldsymbol{g}_h(\boldsymbol{q}_h)$, $\boldsymbol{d}_h(\dot{\boldsymbol{q}}_h)$, $\boldsymbol{k}_h(\dot{\boldsymbol{q}}_h) \in \mathbb{R}^n$ denote the torque vectors associated with the limb's gravity, the energy dissipation, and the elasticity of the musculo-tendon units. When the human is unable to produce the required joint torques, external devices such as a rehabilitative robot or a prosthesis could assist by exerting interaction wrenches at various contact points on the limb. As a result, the dynamics equation (1) changes to

$$\begin{aligned}\boldsymbol{M}_h(\boldsymbol{q}_h)\ddot{\boldsymbol{q}}_h + \boldsymbol{C}_h(\boldsymbol{q}_h, \dot{\boldsymbol{q}}_h)\dot{\boldsymbol{q}}_h + \boldsymbol{g}_h(\boldsymbol{q}_h) \\ + \boldsymbol{d}_h(\dot{\boldsymbol{q}}_h) + \boldsymbol{k}_h(\boldsymbol{q}_h) = \boldsymbol{\tau}_h + \sum_{i=1}^{k} \boldsymbol{J}_{h,i}^T(\boldsymbol{q}_h)\boldsymbol{f}_{\text{ext},i},\end{aligned} \tag{2}$$

where $\boldsymbol{f}_{\text{ext},i} \in \mathbb{R}^m$ denotes the interaction wrench defined in an m-dimensional Cartesian space, acting on the i-th point of contact with the limb. Moreover, $\boldsymbol{J}_{h,i}(\boldsymbol{q}_h) \in \mathbb{R}^{m\times n}$ is the Jacobian matrix corresponding to the i-th contact point, such that

$$\dot{\boldsymbol{x}}_i = \boldsymbol{J}_{h,i}(\boldsymbol{q}_h)\dot{\boldsymbol{q}}_h, \tag{3}$$

where $\boldsymbol{x}_i \in \mathbb{R}^m$ is the location of the i-th contact point in Cartesian space.

B. Robot-Based Work Metric

The musculoskeletal system has three forms of stored energy: kinetic energy, gravitational energy, and elastic energy. We define $T_h \in \mathbb{R}$ as the limb's kinetic energy, where

$$T_h = \frac{1}{2}\dot{\boldsymbol{q}}_h^T \boldsymbol{M}_h(\boldsymbol{q}_h)\dot{\boldsymbol{q}}_h, \tag{4}$$

$U_{g,h} \in \mathbb{R}$ as the gravitational energy such that

$$\boldsymbol{g}_h(\boldsymbol{q}_h) = \frac{\partial U_{g,h}}{\partial \boldsymbol{q}_h} \tag{5}$$

and $U_{k,h} \in \mathbb{R}$ as the stored elastic energy in the musculo-tendon units, where

$$\boldsymbol{k}_h(\boldsymbol{q}_h) = \frac{\partial U_{k,h}}{\partial \boldsymbol{q}_h}. \tag{6}$$

Thus, the overall stored energy $S_h \in \mathbb{R}$ of the human limb becomes

$$S_h = T_h + U_{g,h} + U_{k,h}. \tag{7}$$

Considering (3)–(7), the dynamics equation (2) results in the following power-flow equation:

$$\dot{S}_h + P_{\text{diss}} = P_h + P_{\text{ext}}, \tag{8}$$

where

$$P_{\text{diss}} = \dot{\boldsymbol{q}}_h^T \boldsymbol{d}_h(\dot{\boldsymbol{q}}_h) \geq 0, \tag{9}$$

$$P_h = \dot{\boldsymbol{q}}_h^T \boldsymbol{\tau}_h, \qquad P_{\text{ext}} = \sum_{i=1}^{k} P_{\text{ext},i}, \tag{10}$$

$$P_{\text{ext},i} = \dot{\boldsymbol{q}}_h^T \boldsymbol{J}_{h,i}^T(\boldsymbol{q}_h)\boldsymbol{f}_{\text{ext},i} = \dot{\boldsymbol{x}}_i^T \boldsymbol{f}_{\text{ext},i}. \tag{11}$$

According to (8), the variations in the stored energy S_h result from the summation of the human input power P_h associated with muscle activation as well as the external power P_{ext} from the external devices subtracted by the dissipated power P_{diss}. Figure 1 depicts the port-based modeling of the system. During one motion cycle, the performed work associated with different ports of the system can be described according to (8) as follows:

$$\begin{aligned}S_{h,\text{end}} - S_{h,\text{start}} + E_{\text{diss}} \\ = W_h + W_{\text{ext}},\end{aligned} \tag{12}$$

$$E_{\text{diss}} = \int_{t_{\text{start}}}^{t_{\text{end}}} P_{\text{diss}}\, dt, \quad W_h = \int_{t_{\text{start}}}^{t_{\text{end}}} P_h\, dt, \tag{13}$$

$$W_{\text{ext}} = \int_{t_{\text{start}}}^{t_{\text{end}}} P_{\text{ext}}\, dt = \sum_{i=1}^{k} \int_{t_{\text{start}}}^{t_{\text{end}}} \dot{\boldsymbol{x}}_i^T \boldsymbol{f}_{\text{ext},i}\, dt, \tag{14}$$

where t_{start}, t_{end} are the times and $S_{h,\text{start}}$, $S_{h,\text{end}}$ are the energy values associated with the beginning and the end of the motion cycle, respectively. Considering (4)–(7), the values of $S_{h,\text{start}}$ and $S_{h,\text{end}}$ remain the same for a repetitive motion where the initial and final limb configurations and velocities (i.e., $\boldsymbol{q}_h, \dot{\boldsymbol{q}}_h$) are kept the same for all iterations.[1] Moreover, when the limb's mass is large enough, the magnitude of the kinetic and potential energy is significantly larger than the changes in dissipated energy E_{diss} between steps; thus, the changes in E_{diss} can be considered negligible and the left side of (12) can be assumed constant across iterations. Therefore, we can deduce that any increase/decrease in W_{ext} (i.e., work performed by the robot) for two consecutive cycles is associated with a decrease/increase in W_h (i.e., work performed by the human). In other words, by monitoring the changes in the work performed by the robot according to (14), we can indirectly evaluate the human's active participation in the motion, i.e.,

[1]Please note that we neglect the effect of the musculo-tendon elasticity variation over iterations, which would result in different values of $U_{k,h}$ even for a same configuration $\boldsymbol{q}_h$.

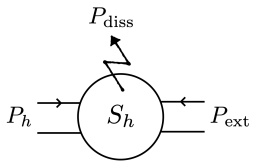

Fig. 1. Port-based modeling of the limb in contact with external devices.

the evolution of W_h. This analysis is the core idea behind our proposed *robot-based work* metric.

Following the concept of *reference energy* as in [40], and by defining $W_{\text{ext}}^{\dagger}$ as the work performed by the interactive robot when the human limb is entirely passive (i.e., for $W_h = 0$), the active participation of the human in the movement can be monitored by iteratively comparing W_{ext} with $W_{\text{ext}}^{\dagger}$. Hence, similar to the observer metric in [40], our robot-based metric for determining the human's (h) contribution during a motion cycle can be defined as

$$\hat{W}_h = W_{\text{ext}}^{\dagger} - W_{\text{ext}}. \tag{15}$$

Obviously, when the human is passive during a motion cycle (i.e., when $W_h = 0$), the value of W_{ext} is identical to $W_{\text{ext}}^{\dagger}$, and considering (15), the *robot-based work* metric $\hat{W}_h$ becomes zero.

C. EMG-Based Work Metric

Muscles convert chemical energy (i.e., ATP) into mechanical work in the form of force generated by the muscle's contractile element (CE). This is also referred to as the *active force* of the muscle, while the *passive force* results from passive stretching of the muscle's viscoelastic elements [41]. In (1), $\boldsymbol{\tau}_h$ represents the torque generated by the active muscle force, whereas the torque vector $\boldsymbol{h}_h(\boldsymbol{q}_h)$ is associated with the energy stored due to passive stretching of the muscle's viscoelastic elements. The total muscle force is the sum of the *active force* generated by the contractile unit and the *passive force* provided by the elastic elements in parallel with the contractile unit [42].

By definition, the work performed by a muscle m must be calculated from the *active force*, $F_{m,a} \in \mathbb{R}$. While there is no way to directly measure this force or the resulting work, it has been well established that EMG activity is correlated with $F_{m,a}$ under certain conditions [43], [44], wherein

$$F_{m,a} = a F_{\max} f(\bar{l}_{mf}, \bar{\dot{l}}_{mf}). \tag{16}$$

Here, $a \in [0, 1]$ is muscle activation, parameter $F_{\max} \in \mathbb{R}_{>0}$ is maximum active muscle force, while $\bar{l}_{mf} \in \mathbb{R}_{>0}$ and $\bar{\dot{l}}_{mf} \in \mathbb{R}$ are normalized muscle fiber length and change rate, respectively. Model $f(\cdot)$ in (16) contains shape parameters for the force-length and the force-velocity curves of skeletal muscle. The detailed equation can be found in [42]. We may estimate the muscle activation a directly from EMG measurement $\tilde{a}$ according to

$$a = \kappa \tilde{a} + \tilde{a}_0, \tag{17}$$

where $\kappa \in \mathbb{R}_{>0}$ is a constant scaling factor and $\tilde{a}_0 \in \mathbb{R}$ is the quiescent EMG baseline. These parameters are unique to each subject, muscle, and sensor placement. If we further assume

Fig. 2. VEMOTION system and setup (Reactive Robotics GmbH).

that the tendon is rigid, we find that $\bar{l}_{mf} = f(\boldsymbol{q}_h)$ and $\bar{\dot{l}}_{mf} = f(\boldsymbol{q}_h, \dot{\boldsymbol{q}}_h)$, making it possible to estimate $F_{m,a}$ from EMG and kinematic data, given parameters κ, $\tilde{a}_0$, and $F_{\max}$.

Considering the sets of agonist muscles M_{ag} and antagonist muscles M_{ant} involved in a given motion, we can estimate the work performed by the human muscles (m) according to

$$\hat{W}_m = \sum_{m \in M_{\text{ag}}} \int_{t_{\text{start}}}^{t_{\text{end}}} F_{m,a} \dot{l}_m dt - \sum_{m \in M_{\text{ant}}} \int_{t_{\text{start}}}^{t_{\text{end}}} F_{m,a} \dot{l}_m dt. \tag{18}$$

Here, $\dot{l}_m \in \mathbb{R}$ is the muscle length change rate, which we can also assume to follow $\dot{l}_m = f(\boldsymbol{q}_h, \dot{\boldsymbol{q}}_h)$. This is similar to the method described in [45] for calculating muscle joint work. Note that we expect $\hat{W}_m \approx \hat{W}_h$ for the same motion, given that the motion trajectory is constrained by the robot.

III. Methods

A. Hardware Setup

The VEMOTION system (figure 2), used in this study, consists of a hospital bed with a harness/seat support system and a robotic attachment for moving the patient's legs through a stepping-like motion. The bed can be tilted to achieve a maximum patient inclination angle of 70°. Each foot is strapped to a footplate, which is free to slide passively along the y-axis as well as to rotate about the z'-axis (figure 2). The z'-axis is perpendicular to the $x-y$ plane, which corresponds with the saggital plane of the patient, but it does not allign with the patient's ankle. The robotic end effectors attach to the patient thighs and follow an arc trajectory in the sagittal plane about the hip joint center, thus moving the patient's legs through a stepping-like motion. Only one leg is moved at a time; the other is held in full extension, i.e., stance phase. Therapy parameters, such as the hip range of motion (ROM) and step frequency, can be set by the clinician.

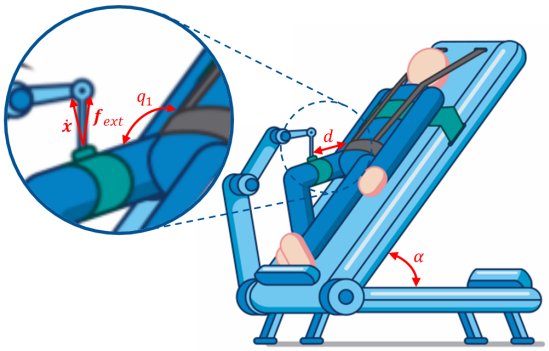

Fig. 3. VEMOTION variables of interest. (Adapted from [24].)

An "assist-as-needed" (AAN) support mode, described in [24], automatically adapts the support level to the patient so that it provides only the required amount of support to enable the patient to move each individual leg along the desired reference trajectory. This is achieved by "shaping" the input velocity of the robotic motion. The AAN setting can be turned on and off as often as required during VEMOTION therapy. When not in use, the patient receives full (100%) support by the robot throughout the motion cycle, meaning that the input velocity curve is fixed.

The VEMOTION system is equipped with various force and link angle sensors, which are used for robot control and safety monitoring as well as for estimating and tracking certain variables of interest. These variables, which are calculated based on the sensor measurements as well as a thigh length measurement d, i.e., the distance between the hip joint center (HJC) and the robot end effector, may be exported from the VEMOTION system after the therapy (written data frequency of 50Hz). In this study, the following variables were of interest: the human-robot interaction wrench vector, $\boldsymbol{f}_{\text{ext}}$, the robot end effector velocity vector, $\dot{\boldsymbol{x}}$, the patient hip flexion angle, q_1, and the bed tilt angle, α (figure 3).

B. Study Participants

1) Healthy Subjects: The metric verification study took place in the Human Motor Control Lab of the Technical University of Munich (TUM). Twelve healthy subjects participated: 7m/5f; 31 ± 4years; 174 ± 11cm; 73 ± 13kg (mean $\pm$ standard deviation). All subjects provided written consent after being informed of the study details. The ethics proposal was submitted to the ethics committee of the TUM and no objections were raised (study number 2022-623-S-KH).

2) Patients: Additional data were collected from two ICU patients of the Schön Klinik Bad Aibling Harthausen (SKBA) who were undergoing VEMOTION-based mobilization as part of their hospital care. Patient 1 was a 79-year-old female (171cm, 77kg) with polytrauma following a traffic accident and suffering from muscle weakness, delirium, dysphagia, and respiratory insufficiency. Patient 2 was an 81-year-old male (170cm, 93kg) with a critical-illness-polyneuropathy/-myopathy following a prolonged ICU stay due to complications from Covid-19. He was suffering from muscle weakness, dysphagia, and respiratory insufficiency. In addition to VEMOTION therapy, the patients also received

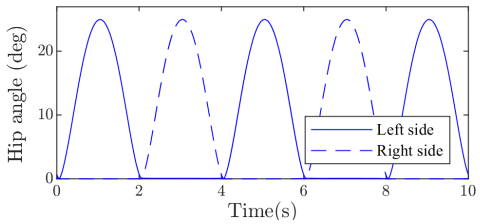

Fig. 4. VEMOTION motion cycle used for healthy subjects.

standard care, including a combination of physiotherapy, occupational therapy, swallowing therapy, neuropsychology, and breathing therapy. The experimental protocol was reviewed by the Ludwig Maximilians University of Munich Ethics Committee under project number 18-645 and no objections were raised.

C. Experimental Protocol

1) Healthy Subjects: Subjects were asked to lay on the VEMOTION bed, after which their thighs and feet were strapped to the robot end effectors and foot plates, respectively, and the seat support was adjusted to their body size. This was in accordance with the manufacturer guidelines. Surface electromyography (sEMG) sensors with integrated accelerometers (Mini Wave Infinity, Cometa Srl, Milan, Italy) were attached to the subjects' skin to measure muscle activity from the left and right m. iliopsoas (IP) at 2kHz, following [46]. In addition, a third sEMG sensor was positioned on the VEMOTION control console and was manually tapped at the beginning and end of each protocol phase for easier post processing and temporal alignment of sEMG and VEMOTION data.

The initialization protocol specified by the manufacturer was followed and the following therapy settings were used: bed tilt angle $\alpha = 50°$, hip flexion/extension range of motion (ROM) $q_1 = 0 - 25°$ (min $-$ max), step frequency $f = 30\text{min}^{-1}$ (figure 4). Each data collection began with a calibration phase, wherein the subject was instructed to relax fully, the VEMOTION was set to full (100%) support, and data were collected from three full left and right steps. After this, the AAN setting was initialized and subjects were instructed to first participate actively for $\sim$ 30s, then to simulate fatigue (i.e., decrease active participation) for $\sim$ 30s, and then return to full active participation for $\sim$ 30s. The same procedure was followed using the standard therapy setting. Note that this experiment was part of a larger data collection protocol, which required a total time of two hours or less, and not all details are specified here.

2) Patients: The patient VEMOTION and sEMG setup protocol was identical to that of the healthy subjects. The therapist selected the robotic end effector ROM according to the patient's hip ROM, q_1. The robot-supported leg movement was started (full support) while the patient bed was horizontal. The therapist gradually adjusted the bed angle α to the highest setting that the patient could tolerate on that day, according to the therapist's professional experience. The final settings were: $\alpha = 30°$ (patient 1), $\alpha = 25°$ (patient 2), $q_1 = 0{-}25°$ (min$-$max; both patients), $f = 20\text{min}^{-1}$ (both patients).

Four active trials were performed per patient; two with the full support setting and two with the AAN setting (in

alternating order, beginning with full support). For each trial, the patient was encouraged to actively follow the stepping motion of the robot end effector with his/her legs as much as possible. Care was taken to ensure that the instructions given to the patient were consistent between therapy types. After approximately one minute, corresponding to between 8−16 steps per leg, the patient was allowed to relax and, in the case of the AAN trials, the full support setting was resumed. The patient was allowed a 2−3 minute break between each active trial. After all trials were completed, the bed angle was returned to horizontal and the therapy was ended.

D. Evaluation Metrics

1) Robot-Based Work Metric: For each step of the therapy, we estimated the *robot-based work* metric for the hip flexion and extension phases separately, referred to as $\hat{W}_{h,f}$ and $\hat{W}_{h,e}$, respectively. The calculation, which follows section II-B, is described in the paragraphs below. It may be noted that these phases were chosen because, due to the sinusoidal rehabilitation motion (figure 4), joint velocities $\dot{\boldsymbol{q}}_h = \mathbf{0}$ at the beginning and end of flexion and extension and the initial and final configurations $\boldsymbol{q}_h$ remain the same across the iterations. Thus, $S_{h,\text{start}}$ and $S_{h,\text{end}}$ could safely be assumed to remain constant throughout the motion cycles. In fact, these energy values are only associated with the limb's gravity $\boldsymbol{g}_h(\boldsymbol{q}_h)$ and the muscle elasticity $\boldsymbol{h}_h(\boldsymbol{q}_h)$; see section II-B.

The physical interaction between the VEMOTION robot and the human was described through one contact point, for the sake of simplicity. Thus, considering (14), the work performed by the robot during the flexion phase was estimated as

$$W_{\text{ext},f} = \int_{t_{\text{start},f}}^{t_{\text{end},f}} P_{\text{ext}}\, dt = \int_{t_{\text{start},f}}^{t_{\text{end},f}} \dot{\boldsymbol{x}}^T \boldsymbol{f}_{\text{ext}}\, dt, \tag{19}$$

where $t_{\text{start},f}$ and $t_{\text{end},f}$ correspond to the flexion start and end index, respectively, for the given step. The reference energy $W^{\dagger}_{\text{ext},f}$ was determined during the calibration phase, i.e., when the human is passive ($W_{h,f} = 0$). Finally, the *robot-based work* for the flexion phase was derived according to (15) as

$$\hat{W}_{h,f} = W^{\dagger}_{\text{ext},f} - W_{\text{ext},f}. \tag{20}$$

The same process was followed for estimating the extension phase variables $\hat{W}_{h,e}$, $W^{\dagger}_{\text{ext},e}$, and $W_{\text{ext},e}$.

2) EMG-Based Work Metric: An important consideration for the *EMG-based work* metric introduced in section II-C was the muscle selection for measurement. Due to the kinematic constraint at the foot in the VEMOTION system, flexion (or extension) of the hip and knee joints are forced to be coupled, thus rendering the bi-articular muscles, i.e., m. rectus femoris (RF) and m. biceps femoris (BF), less effective than during normal gait. In fact, it was observed in our previous work that the activation patterns of these muscles is highly inconsistent (between subjects) during VEMOTION therapy, even for healthy subjects [48]. Based on this evidence as well as preliminary experiments, we assumed in this work that the stepping motion is primarily driven by hip flexion- and extension-specific muscles, i.e. single-joint muscles. Surface EMG measurement of hip extensors, e.g. m. gluteus maximus,

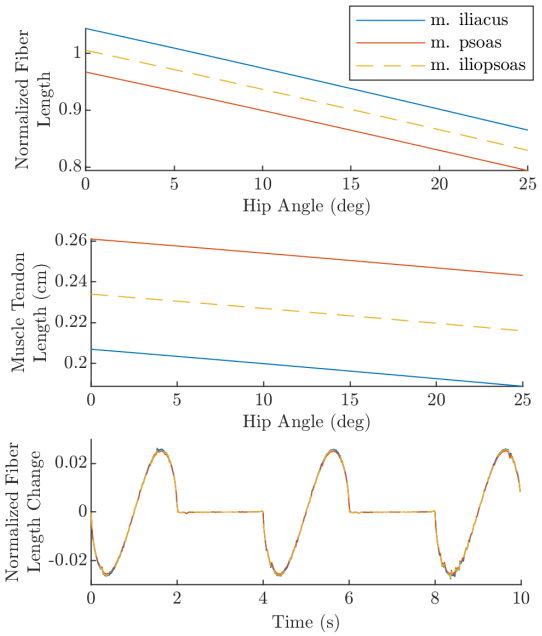

Fig. 5. Normalized muscle fiber length ($\bar{l}_{mf}$) and muscle-tendon length (l_m) of the m. iliacus and m. psoas vs. hip flexion angle over the range of motion used in this study. Normalized muscle fiber length change ($\bar{\dot{l}}_{mf}$) is also shown for both muscles for three motion cycles. Here, the negative length change corresponds to the hip flexion phase and the positive length change corresponds to the hip extension phase. Plotted results are based on a state-of-the-art musculoskeletal model [47].

was not feasible with the VEMOTION setup. Therefore, the focus here was to estimate the hip flexion work by measuring EMG from an accessible hip flexion-specific muscle group, i.e. the m. iliopsoas (IP) [46]. For practical purposes, this also required us to assume minimal co-activation of the antagonist muscles during hip flexion. As a result, we will refer to $\hat{W}_m$ for the flexion phase as $\hat{W}_{m,IP}$ from here on.

A preliminary evaluation of the m. iliacus and the m. psoas muscles with a state-of-the-art musculoskeletal model [47] shows that $\bar{l}_{mf,IP} \in [0.83, 1.0]$ and $\bar{\dot{l}}_{mf,IP} \in [-0.026, 0]$ for the lumped IP, given the hip flexion motion cycle ($q_1(t)$; figure 5). Recall that we assumed a rigid tendon, so that $\bar{l}_{mf,IP}$ and $\bar{\dot{l}}_{mf,IP}$ may be directly estimated from hip flexion $q_1(t)$.

Further, we estimated $\tilde{a}$, introduced in (17), directly from the root mean square (RMS) of the m. iliopsoas sEMG measurement. At this stage, the values of parameters κ, $\tilde{a}_0$, and $F_{\max}$ were unknown for a given muscle and sensor setup. However, given that the flexion motion is (primarily) driven by the m. iliopsoas, i.e. a single muscle group, the correlation between $\hat{W}_{h,f}$ and $\hat{W}_{m,IP}$ is minimally affected by the choice of parameters.[2] Thus, in a first step we calculated an intermediate version of the *EMG-based work* metric according to (16) and (18), which we refer to as $\hat{W}^*_{m,IP}$, where

$$\hat{W}^*_{m,IP} = \int_{t_{\text{start,f}}}^{t_{\text{end,f}}} \tilde{a}\, f(\bar{l}_{mf,IP}, \bar{\dot{l}}_{mf,IP}) \dot{l}_{m,IP} dt. \tag{21}$$

[2]This only holds true for a given muscle and sensor setup. A more precise estimate of κ, $\tilde{a}_0$, and $F_{\max}$ are required for inter-subject comparison.

Note that this is equivalent to arbitrarily assuming that $\kappa = 1$, $\tilde{a}_0 = 0$, and $F_{\max} = 1$. Here we used the standard shape parameters reported in the Github repository for [42].[3]

In a second step, we estimated $\kappa F_{\max}$ and $\tilde{a}_0 F_{\max}$ for each subject and side by assuming $\hat{W}_{h,f} = \hat{W}_{m,IP}$. For this, first (16) and (17) were substituted into (18). Defining

$$\Gamma = f(\bar{l}_{mf,IP}, \bar{\dot{l}}_{mf,IP})\dot{l}_{m,IP}, \tag{22}$$

the resulting equation was then reformulated as

$$\hat{W}_{m,IP} = \kappa F_{\max} \underbrace{\int_{t_{\text{start,f}}}^{t_{\text{end,f}}} \tilde{a}\Gamma dt}_{\hat{W}^*_{m,IP}} + \tilde{a}_0 F_{\max} \int_{t_{\text{start,f}}}^{t_{\text{end,f}}} \Gamma dt. \tag{23}$$

Using the data set (i.e., all steps) from each subject and side separately, linear regression was then used to estimate $\kappa F_{\max}$ and $\tilde{a}_0 F_{\max}$, corresponding to that muscle and sensor setup. Finally, $\hat{W}_{m,IP}$ was calculated for each subject (healthy or patient), side, therapy type, and step.

E. Data Analysis

All data were processed and analyzed using a custom Matlab script (The MathWorks, Natick, MA, USA). For the statistical analysis, the statistics and machine learning toolbox was used. The force data were filtered using a moving average window (size 220ms), signal bias was removed, and the filter time shift was compensated. The sEMG sensors used have a built-in band-pass filter ($5-500$Hz, 3dB/oct, 4th order). The signals were full-wave rectified and the moving window root mean square (RMS) was calculated (200ms window size).

VEMOTION data (α, q_1, $\boldsymbol{f}_{\text{ext}}$, and $\dot{\boldsymbol{x}}$) and EMG data were synchronized in a two-step process. Approximate alignment was achieved using the manual "tap" signals from the sEMG sensor and the manual "start" signals from the VEMOTION data log. Precise synchronization (within ~ 20ms) was achieved by aligning the leg motion profiles measured by the sEMG-integrated accelerometer and the VEMOTION angle sensors. The "tap" signals also served to define start and stop indices of each therapy phase. Finally, indices for the beginning and end of the flexion and extension phases were identified for each step, based on the motion profiles.

The *robot-based work* metrics $\hat{W}_{h,f}$ and $\hat{W}_{h,e}$ were calculated for each subject (healthy or patient), side, therapy type, and step according to (19)-(20). The pseudo and final *EMG-based work* metrics $\hat{W}^*_{m,IP}$ and $\hat{W}_{m,IP}$ were similarly calculated according to (21)-(23). The coefficient of determination, R^2, was then calculated between $\hat{W}_{h,f}$ and $\hat{W}^*_{m,IP}$ for each subject and side individually. Finally, R^2 was calculated between $\hat{W}_{h,f}$ and $\hat{W}_{m,IP}$ for the combined data of all subjects. Therapy types were assessed separately. Individual patient trials were also assessed separately. Outliers were identified as any data point lying more than $1.5 \cdot IQR$ (interquartile range) outside of the first or third quartile. These data points were excluded from the summary statistics, though they are shown in the plots. Additionally, one healthy subject's AAN therapy data were excluded from the analysis due to a safety-related hardware shutdown before the end of the trial.

[3]https://github.com/mjhmilla/Millard2012EquilibriumMuscleMatlabPort

IV. Results

A. Verifying the Work Metrics

The coefficient of determination (R^2) between $\hat{W}^*_{m,IP}$ and $\hat{W}_{h,f}$ of the healthy subject data, assessed for each subject individually, ranged from 0.43 to 0.99 (excluding outliers) for the standard therapy and from 0.44 to 0.95 for the AAN therapy ($p < 0.01$). Similar results were observed in the patient data. Specifically, R^2 ranged from 0.39 to 0.97 for the standard therapy and from 0.55 to 0.95 (excluding the outlier) for the AAN therapy ($p < 0.05$). See figure 6. The results were identical when comparing $\hat{W}_{m,IP}$ and $\hat{W}_{h,f}$.

When the $\hat{W}_{m,IP}$ and $\hat{W}_{h,f}$ data were combined for all twelve healthy subjects, R^2 was found to be 0.93 for the standard therapy case (excluding data from the three outlier trials seen in figure 6) and 0.86 for the AAN therapy case ($p < 0.001$). For the combined patient data, R^2 was 0.77 for the standard therapy data and was 0.92 for the AAN therapy data ($p < 0.001$, excluding data from the outlier trial seen in figure 6). See figure 7.

For further verification, the two work metrics are shown for a representative example of a healthy subject AAN trial (figure 8). During the phases when the subject was instructed to be passive, the work performed by the subject, estimated by both $\hat{W}_{m,IP}$ and $\hat{W}_{h,f}$, is very low. During the phases when the subject was instructed to participate actively, the work, as estimated with each of the independent metrics, increases with each step. Similar results were found for all subjects.

B. Comparing $\mathbf{W}_{\text{h}}$ Between Standard and AAN Therapy

The distribution of $W_{h,f}$ and $W_{h,e}$ across steps is shown for each patient, side, and therapy trial in figures 9 and 10, respectively. Positive values may be interpreted as the patient performing work in the direction of the motion (referred to as "positive work"). Negative results may be interpreted as patient performing work against the direction of motion, i.e., the patient resisting the motion driven by the robot (referred to as "negative work"). Values near zero may be interpreted as the patient behaving passively, i.e., minimal muscle activation. (See equation (20).)

It can be observed from these results that both patients performed primarily positive work in the flexion phase and primarily negative work in the extension phase. The exception is patient 1, who was relatively passive in the extension phase of the standard therapy trials. Furthermore, patient 2 performed a higher magnitude of positive work than patient 1 in the flexion phase and a higher magnitude of negative work in the extension phase, but did not achieve the same peak magnitude as was observed in the healthy subjects.

The difference in $W_{h,f}$ and $W_{h,e}$ between standard therapy and AAN therapy is not very pronounced in general. Notably, however, there is a large increase in positive flexion work between the standard and AAN therapy 1 for patient 1.

V. Discussion

Voluntary drive is critical during patient rehabilitation therapy, in order to optimize recovery, and robotic systems are promising tools for this purpose. However, it is difficult to estimate the human contribution during shared human-robot tasks

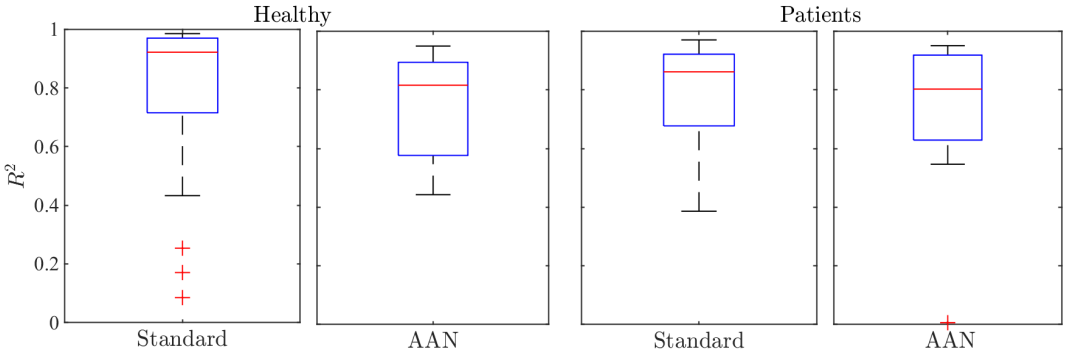

Fig. 6. Distribution statistics of the correlation between $\hat{W}^*_{m,IP}$ and $\hat{W}_{h,f}$, quantified for each subject, side, and trial individually. Outliers are indicated with red crosses.

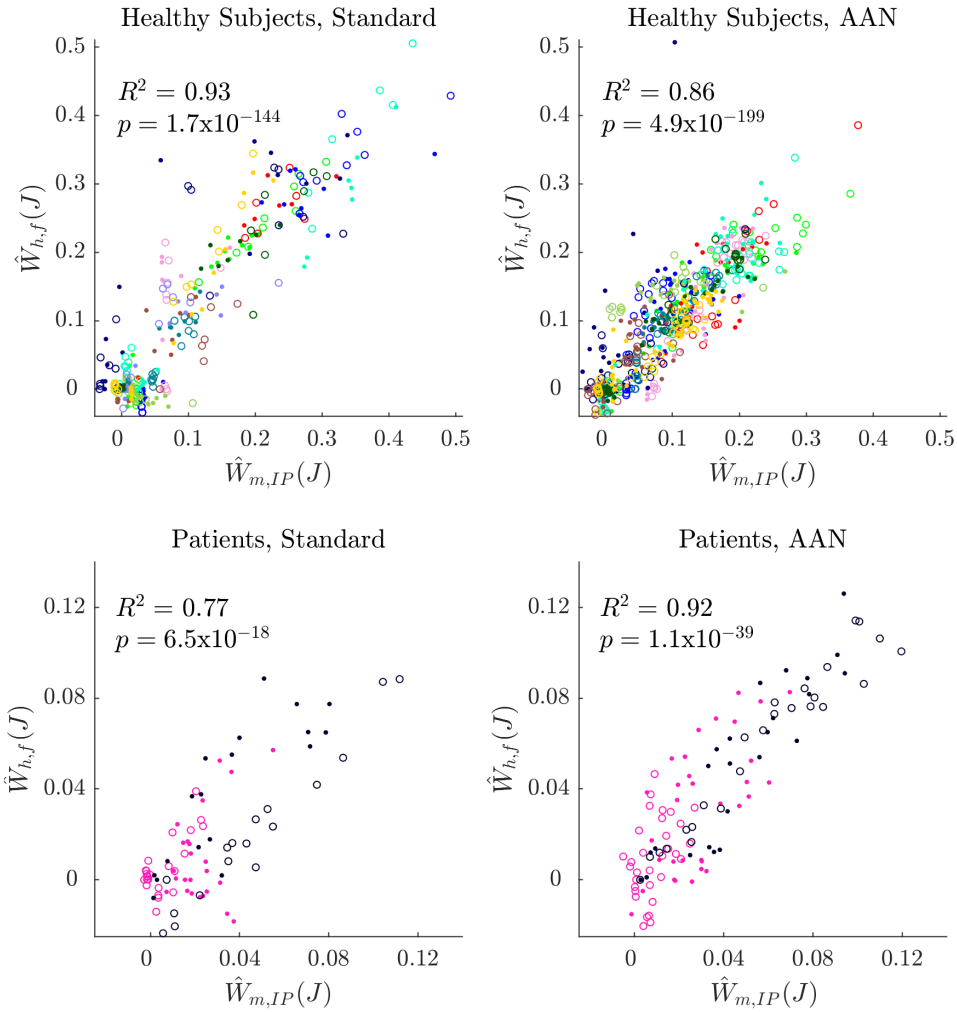

Fig. 7. Comparison between $\hat{W}_{m,IP}$ and $\hat{W}_{h,f}$ for all steps of all healthy subjects and patients using the standard therapy and the AAN therapy settings. Each subject is represented by a single color (right leg data is depicted with closed circles, left leg with open circles).

without the use of body-worn sensors. Various biomechanical measures have been introduced, but, to the knowledge of the authors, none has been systematically evaluated and verified. In this paper, we have presented two metrics for quantifying the work performed by a patient during robot-assisted lower extremity rehabilitation and we have tested and verified them against each other using both healthy subject and patient data sets. The two metrics, $\hat{W}_h$ and $\hat{W}_m$, calculated from independent sensor measurements following different computational models, have identical biomechanical interpretability, meaning that the values should be equal. Thus, by comparing the quantified measures, the validity of the metrics may be evaluated. Indeed, the results show a strong correlation between the two measures. Although the best test of validity, i.e., comparison against ground truth, was not feasible, the presented results further demonstrate consistency between the outcome measures and the instructions given to the subjects. Based on these combined results, we conclude that there is

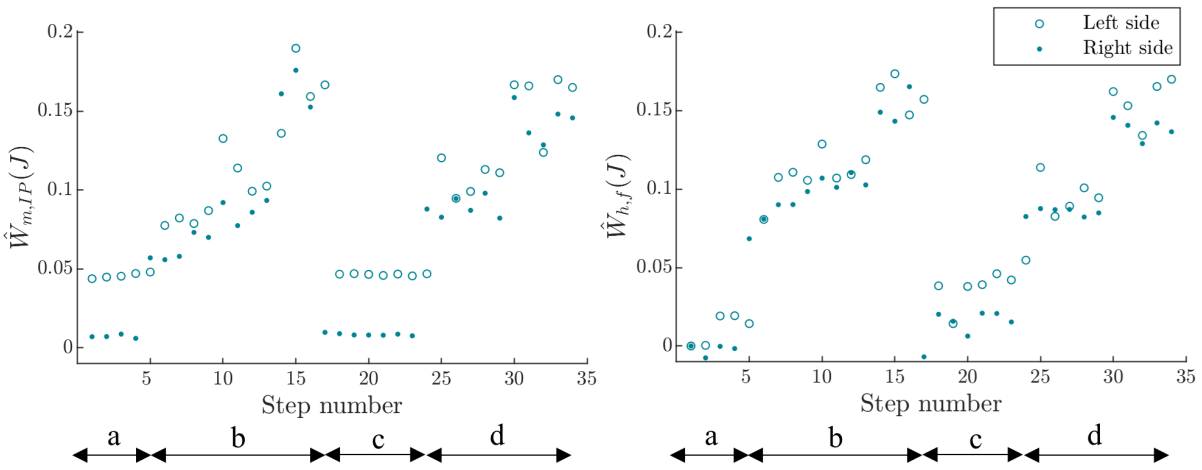

Fig. 8. Example $\hat{W}_{m,IP}$ and $\hat{W}_{h,f}$ results from one healthy subject performing the AAN trial. In phases (**a**, calibration phase) and (**c**), the subject was instructed to be passive and let the robot do the work. In phases (**b**) and (**d**), the subject was instructed to participate actively.

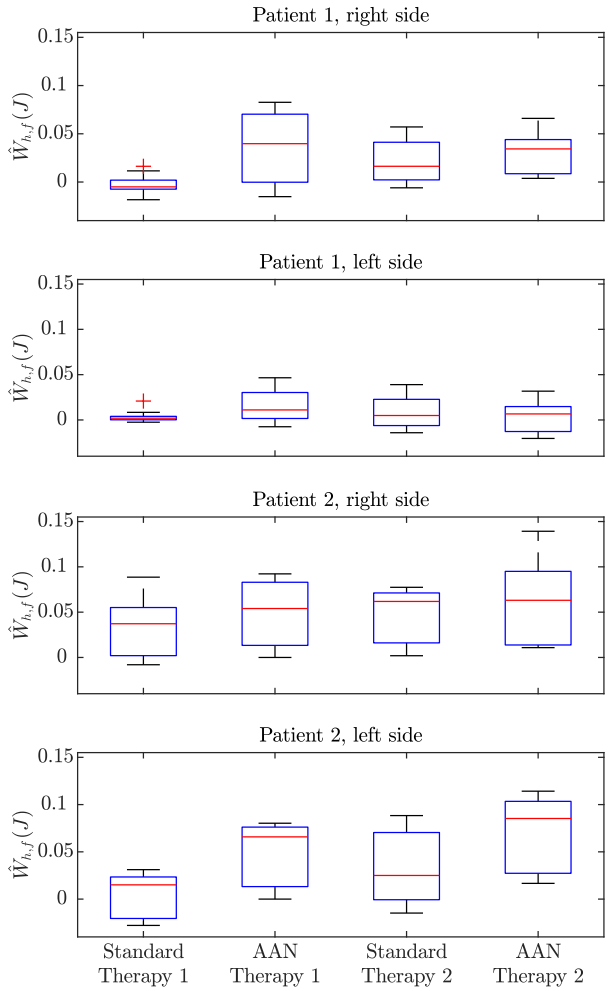

Fig. 9. Flexion work performed by the patients during each trial.

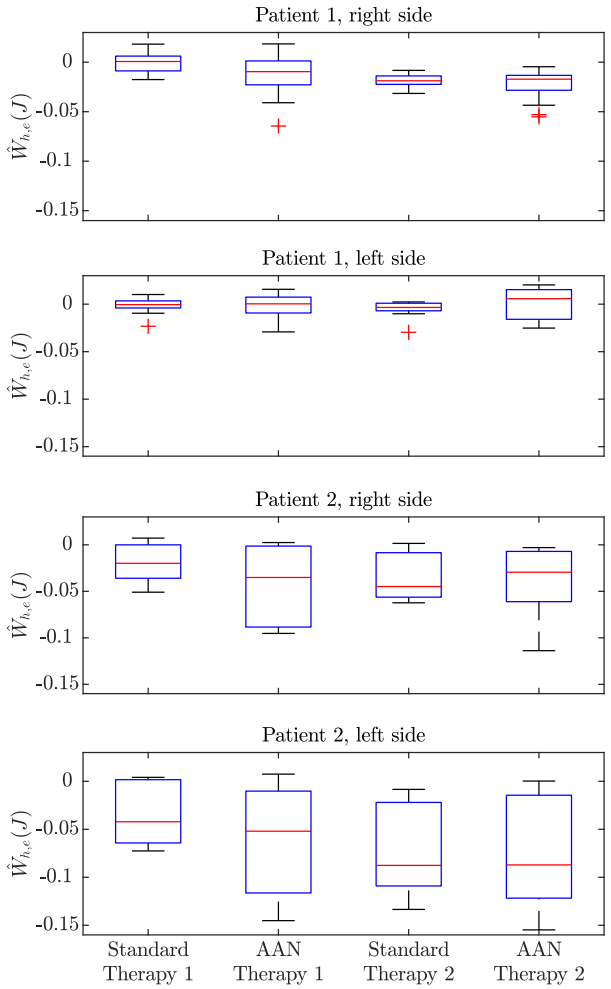

Fig. 10. Extension work performed by the patients during each trial.

strong evidence that both metrics serve as valid estimators of the productive work done by the human (muscles). The results further support that the metrics are not only valid with 100% support mode, but with a reduced assistance level, which has previously been considered particularly challenging for estimates based solely on interaction force measurements [26]. This outcome was expected because both metrics integrate measurements (or estimates) of both force and motion. It may be additionally noted that the metrics are agnostic to the type of (AAN) control algorithm used, because no assumptions were made with regard to the control algorithm.

While many different aspects of work could have been considered, we chose in this study to focus on what we refer to as "productive" work as a quantitative estimate of the

patient's active participation during the mobilization therapy. Other metrics, such as those described in [26], [31], [32], [33], [34], [35], [36], [37], and [38], may be better for evaluating the quality of the patient's muscle coordination, for example. Developing better methods for assessing quality of movement would be an important extension of this work. For example, erratic movements can result in an increased effort from the patient, which is undesirable.

An interesting aspect of the two chosen metrics is that one is calculated in Cartesian space while the other is calculated in muscle space, yet, the final result has the same physical meaning for both. This was possible due to the strategic choice to quantify work (as opposed to force) produced by the human. Quantifying work meant that no model-based mapping (e.g., Jacobian) was required in order to convert from one space to another, making the comparison feasible. Furthermore, for the given setup (i.e., constrained motion. which is primarily driven by a single muscle group), the corresponding metrics made it possible to calibrate the EMG-force relationship, which generally requires the use of relatively unreliable maximum voluntary contraction experiments [49]. Thus, the presented method also represents an interesting alternative for EMG calibration under certain circumstances.

In this work, we additionally performed a preliminary comparison between patient participation during a standard (full robotic support) therapy vs. an assist-as-needed therapy setting. While there is not a statistically significant difference in the distributions between the standard therapy and the AAN therapy settings, we do see some interesting results for each patient. In the first standard therapy trial, patient 1 was almost fully passive, despite being directed to actively participate in the leg movement. This patient was in an altered mental state. In the subsequent trial the AAN setting was used and we observe a large increase in the patient's $\hat{W}_{h,f}$, indicating that she was able to actively participate. Notably, this increased activity level persisted for the subsequent standard and AAN trials. One possibility to consider is that the AAN trial may have enabled the patient to remember the motor activation patterns and that this memory persisted. This could indicate that the adaptive support level during AAN therapy served as a kind of biofeedback to the patient, which is believed to be important for effective rehabilitation [50]. However, these assertions cannot be verified from the current data. A larger study is needed in which the first trial is randomized between standard and AAN therapy in order to address this question.

In patient 2, the data show an upward shift of the 75th percentile and maximum $\hat{W}_{h,f}$ as well as a downward shift of the 25th percentile and minimum $\hat{W}_{h,e}$ when comparing AAN to standard therapy. This patient was much more cognitively fit. While the $\hat{W}_{h,f}$ data show an encouraging trend, the negative $\hat{W}_{h,e}$ results point to the hip flexor providing active resistance during the extension phase, which is not desired. Further investigation revealed that the problem may arise due to the extension velocity during AAN therapy being too high. Thus, the metric enables useful assessment of the effect of various control strategies on the patient performance.

An important consideration when using the presented work metrics is that patient activity level and performance are not only related to neuromuscular impairment, but also effort, cognitive impairment, and fatigue state [51], [52], [53]. While the above described measures give an estimate of patient activity and physical performance, extending the method to include psychophysiological parameters may provide a way to distinguish whether poor performance is due to lack of effort, fatigue, or true physical limitation. One reason this is important is because it has been observed that full robotic support during therapy can lead to effort reduction, likely due to the lack of movement error [52].

The main limitation of this work is that only the flexion phase could be validated due to limitations of muscles from which sEMG could be measured. It is also important to note that, based on the sEMG sensor placement, it is possible that some signal was coming from the proximal m. rectus femoris. It has been previously shown that the muscle activity measured from the proximal RF is hip flexion-specific [54]; thus, the current results are likely not negatively impacted by this potential cross talk.

VI. Conclusion

The results of this work demonstrate, on the basis of twelve healthy subject and two patient data sets, that the presented robot-based and EMG-based metrics are both valid estimates of the work performed by a patient during robotic rehabilitation therapy. Given that only robot-integrated sensors are required for the *robot-based work* metric, this is an excellent option for application in an ICU or general hospital setting when used in conjunction with a robot specifically designed for this setting. Thus, the *robot-based work* metric may be useful for evaluating the effectiveness of AAN in appropriately challenging the patient during a therapy session.

Acknowledgment

The authors would like to thank Alisa Buetikofer and Martina Steinböck for their support in patient data collection and manuscript review.

References

[1] K. J. Stuempfle and D. G. Drury, "The physiological consequences of bed rest," *J. Exerc. Physiol.*, vol. 10, no. 3, pp. 32–41, 2007.
[2] V. A. Convertino, "Cardiovascular consequences of bed rest: Effect on maximal oxygen uptake," *Med. Sci. Sports Exerc.*, vol. 29, no. 2, pp. 191–196, Feb. 1997.
[3] I. Vanhorebeek, N. Latronico, and G. Van den Berghe, "ICU-acquired weakness," *Intensive Care Med.*, vol. 46, no. 4, pp. 637–653, 2020.
[4] D. Dittmer and R. Teasell, "Complications of immobilization and bed rest. Part 1: Musculoskeletal and cardiovascular complications," *Can. Family Physician*, vol. 39, p. 1428, Jun. 1993.
[5] C. L. Kramer, "Intensive care unit-acquired weakness," *Neurologic Clinics*, vol. 35, no. 4, pp. 723–736, 2017.
[6] G. Hermans and G. Van den Berghe, "Clinical review: Intensive care unit acquired weakness," *Crit. Care*, vol. 19, no. 1, pp. 1–9, Dec. 2015.
[7] G. Hermans et al., "Acute outcomes and 1-year mortality of intensive care unit-acquired weakness. A cohort study and propensity-matched analysis," *Amer. J. Respiratory Crit. Care Med.*, vol. 190, no. 4, pp. 410–420, 2014.
[8] S. N. Fletcher et al., "Persistent neuromuscular and neurophysiologic abnormalities in long-term survivors of prolonged critical illness," *Crit. Care Med.*, vol. 31, no. 4, pp. 1012–1016, Apr. 2003.
[9] S. V. Desai, T. J. Law, and D. M. Needham, "Long-term complications of critical care," *Crit. Care Med.*, vol. 39, no. 2, pp. 371–379, Feb. 2011.

[10] D. M. Needham, "Mobilizing patients in the intensive care unit: Improving neuromuscular weakness and physical function," *Jama*, vol. 300, no. 14, pp. 1685–1690, 2008.

[11] L. Zhang et al., "Early mobilization of critically ill patients in the intensive care unit: A systematic review and meta-analysis," *PLoS ONE*, vol. 14, no. 10, Oct. 2019, Art. no. e0223185.

[12] T. Bein et al., "S2e-leitlinie: Lagerungstherapie und frühmobilisation zur prophylaxe oder therapie von pulmonalen funktionsstörungen: Revision 2015: S2e-leitlinie der deutschen gesellschaft für anästhesiologie und intensivmedizin (dgai)," *Der Anaesthesist*, vol. 64, pp. 1–26, Jan. 2015.

[13] G. Morone et al., "Robot-assisted gait training for stroke patients: Current state of the art and perspectives of robotics," *Neuropsychiatric Disease Treatment*, vol. 13, pp. 1303–1311, May 2017.

[14] J. Laut, M. Porfiri, and P. Raghavan, "The present and future of robotic technology in rehabilitation," *Current Phys. Med. Rehabil. Rep.*, vol. 4, no. 4, pp. 312–319, Dec. 2016.

[15] S. M. Parry and Z. A. Puthucheary, "The impact of extended bed rest on the musculoskeletal system in the critical care environment," *Extreme Physiol. Med.*, vol. 4, no. 1, pp. 1–8, Dec. 2015.

[16] M. Egger, M. Steinböck, E. Shahriari, and F. Müller, "Robotergestützte mobilisierungstherapie mit künstlicher intelligenz," *Neuroreha*, vol. 13, no. 1, pp. 27–31, 2021.

[17] S. M. Dirkes and C. Kozlowski, "Early mobility in the intensive care unit: Evidence, barriers, and future directions," *Crit. Care Nurse*, vol. 39, no. 3, pp. 33–42, Jun. 2019.

[18] K. Stiller, "Safety issues that should be considered when mobilizing critically ill patients," *Crit. Care Clinics*, vol. 23, no. 1, pp. 35–53, Jan. 2007.

[19] R. Dubb et al., "Barriers and strategies for early mobilization of patients in intensive care units," *Ann. Amer. Thoracic Soc.*, vol. 13, no. 5, pp. 724–730, May 2016.

[20] C. Amidei, "Mobilisation in critical care: A concept analysis," *Intensive Crit. Care Nursing*, vol. 28, no. 2, pp. 73–81, Apr. 2012.

[21] R. van den Brand et al., "Restoring voluntary control of locomotion after paralyzing spinal cord injury," *Science*, vol. 336, no. 6085, pp. 1182–1185, Jun. 2012.

[22] A. Duschau-Wicke, J. von Zitzewitz, A. Caprez, L. Lunenburger, and R. Riener, "Path control: A method for patient-cooperative robot-aided gait rehabilitation," *IEEE Trans. Neural Syst. Rehabil. Eng.*, vol. 18, no. 1, pp. 38–48, Feb. 2010.

[23] W. Meng, Q. Liu, Z. Zhou, Q. Ai, B. Sheng, and S. Xie, "Recent development of mechanisms and control strategies for robot-assisted lower limb rehabilitation," *Mechatronics*, vol. 31, pp. 132–145, Oct. 2015.

[24] E. Shahriari, D. Zardykhan, A. Koenig, E. Jensen, and S. Haddadin, "Energy-based adaptive control and learning for patient-aware rehabilitation," in *Proc. IEEE/RSJ Int. Conf. Intell. Robots Syst. (IROS)*, Nov. 2019, pp. 5671–5678.

[25] M. Egger, M. Steinbock, V. Huge, and F. Muller, "An innovative robotic device for early mobilization in the intensive care unit," in *Proc. ntensive Care Med. Exp. Conf., Eur. Soc. Intensive Care Med. Annu. Congr. (ESICM) Digit.*, vol. 9, 2021.

[26] R. Banz, M. Bolliger, G. Colombo, V. Dietz, and L. Lünenburger, "Computerized visual feedback: An adjunct to robotic-assisted gait training," *Phys. Therapy*, vol. 88, no. 10, pp. 1135–1145, Oct. 2008.

[27] L. Marchal-Crespo and D. J. Reinkensmeyer, "Review of control strategies for robotic movement training after neurologic injury," *J. NeuroEng. Rehabil.*, vol. 6, no. 1, pp. 1–15, Dec. 2009.

[28] J. Wagner, T. Solis-Escalante, P. Grieshofer, C. Neuper, G. Müller-Putz, and R. Scherer, "Level of participation in robotic-assisted treadmill walking modulates midline sensorimotor EEG rhythms in able-bodied subjects," *NeuroImage*, vol. 63, no. 3, pp. 1203–1211, Nov. 2012.

[29] A. U. Pehlivan, D. P. Losey, C. G. Rose, and M. K. O'Malley, "Maintaining subject engagement during robotic rehabilitation with a minimal assist-as-needed (mAAN) controller," in *Proc. Int. Conf. Rehabil. Robot. (ICORR)*, Jul. 2017, pp. 62–67.

[30] R. Pilkar, K. Momeni, A. Ramanujam, M. Ravi, E. Garbarini, and G. F. Forrest, "Use of surface EMG in clinical rehabilitation of individuals with SCI: Barriers and future considerations," *Frontiers Neurol.*, vol. 11, Dec. 2020, Art. no. 578559.

[31] K. Gui, U.-X. Tan, H. Liu, and D. Zhang, "Electromyography-driven progressive assist-as-needed control for lower limb exoskeleton," *IEEE Trans. Med. Robot. Bionics*, vol. 2, no. 1, pp. 50–58, Feb. 2020.

[32] J.-I. Furukawa, T. Noda, T. Teramae, and J. Morimoto, "Estimating joint movements from observed EMG signals with multiple electrodes under sensor failure situations toward safe assistive robot control," in *Proc. IEEE Int. Conf. Robot. Autom. (ICRA)*, May 2015, pp. 4985–4991.

[33] T. Teramae, T. Noda, and J. Morimoto, "EMG-based model predictive control for physical human–robot interaction: Application for assist-as-needed control," *IEEE Robot. Autom. Lett.*, vol. 3, no. 1, pp. 210–217, Jan. 2018.

[34] L. Lünenburger, G. Colombo, and R. Riener, "Biofeedback for robotic gait rehabilitation," *J. NeuroEng. Rehabil.*, vol. 4, no. 1, pp. 1–11, Dec. 2007.

[35] Q.-T. Dao and S.-I. Yamamoto, "Assist-as-needed control of a robotic orthosis actuated by pneumatic artificial muscle for gait rehabilitation," *Appl. Sci.*, vol. 8, no. 4, p. 499, Mar. 2018.

[36] M. G. Carmichael and D. Liu, "Estimating physical assistance need using a musculoskeletal model," *IEEE Trans. Biomed. Eng.*, vol. 60, no. 7, pp. 1912–1919, Jul. 2013.

[37] D. Novak et al., "Psychophysiological responses to robotic rehabilitation tasks in stroke," *IEEE Trans. Neural Syst. Rehabil. Eng.*, vol. 18, no. 4, pp. 351–361, Aug. 2010.

[38] E. Papaleo, L. Zollo, L. Spedaliere, and E. Guglielmelli, "Patient-tailored adaptive robotic system for upper-limb rehabilitation," in *Proc. IEEE Int. Conf. Robot. Autom.*, May 2013, pp. 3860–3865.

[39] H. I. Krebs et al., "Rehabilitation robotics: Performance-based progressive robot-assisted therapy," *Autonom. Robot.*, vol. 15, no. 1, pp. 7–20, Jul. 2003.

[40] E. Shahriari, A. Kramberger, A. Gams, A. Ude, and S. Haddadin, "Adapting to contacts: Energy tanks and task energy for passivity-based dynamic movement primitives," in *Proc. IEEE-RAS 17th Int. Conf. Humanoid Robot. (Humanoids)*, Nov. 2017, pp. 136–142.

[41] A. V. Hill, "The heat of shortening and the dynamic constants of muscle," *Proc. Roy. Soc. London. Ser. B, Biol. Sci.*, vol. 126, no. 843, pp. 136–195, Oct. 1938.

[42] M. Millard, T. Uchida, A. Seth, and S. L. Delp, "Flexing computational muscle: Modeling and simulation of musculotendon dynamics," *J. Biomechanical Eng.*, vol. 135, no. 2, Feb. 2013, Art. no. 021005.

[43] T. Y. Fukuda et al., "Root mean square value of the electromyographic signal in the isometric torque of the quadriceps, hamstrings and brachial biceps muscles in female subjects," *J. Appl. Res.*, vol. 10, no. 1, pp. 32–39, 2010.

[44] C. Disselhorst-Klug, T. Schmitz-Rode, and G. Rau, "Surface electromyography and muscle force: Limits in sEMG-force relationship and new approaches for applications," *Clin. Biomechanics*, vol. 24, no. 3, pp. 225–235, Mar. 2009.

[45] K. Sasaki, R. R. Neptune, and S. A. Kautz, "The relationships between muscle, external, internal and joint mechanical work during normal walking," *J. Experim. Biol.*, vol. 212, no. 5, pp. 738–744, Mar. 2009.

[46] T. Jiroumaru, T. Kurihara, and T. Isaka, "Measurement of muscle length-related electromyography activity of the hip flexor muscles to determine individual muscle contributions to the hip flexion torque," *SpringerPlus*, vol. 3, no. 1, pp. 1–9, Dec. 2014.

[47] S. L. Delp et al., "OpenSim: Open-source software to create and analyze dynamic simulations of movement," *IEEE Trans. Biomed. Eng.*, vol. 54, no. 11, pp. 1940–1950, Nov. 2007.

[48] K. K. Peper et al., "Testing robot-based assist-as-needed therapy for improving active participation of a patient during early neurorehabilitation: A case study," in *Proc. Int. Conf. Rehabil. Robot. (ICORR)*, Jul. 2022, pp. 1–6.

[49] D. Staudenmann, K. Roeleveld, D. F. Stegeman, and J. H. van Dieen, "Methodological aspects of SEMG recordings for force estimation—A tutorial and review," *J. Electromyogr. Kinesiol.*, vol. 20, no. 3, pp. 375–387, Jun. 2010.

[50] H. Huang, S. L. Wolf, and J. He, "Recent developments in biofeedback for neuromotor rehabilitation," *J. NeuroEng. Rehabil.*, vol. 3, no. 1, pp. 1–12, Dec. 2006.

[51] E. Ödemiş and C. V. Baysal, "Development of a participation assessment system based on multimodal evaluation of user responses for upper limb rehabilitation," *Biomed. Signal Process. Control*, vol. 70, Sep. 2021, Art. no. 103066.

[52] L. Zimmerli, "Increasing engagement during robot-aided motor rehabilitation using augmented feedback exercices," Ph.D. dissertation, ETH Zurich, 2013.

[53] A. Koenig et al., "Controlling patient participation during robot-assisted gait training," *J. NeuroEng. Rehabil.*, vol. 8, no. 1, p. 14, 2011.

[54] K. Watanabe, T. M. Vieira, A. Gallina, M. Kouzaki, and T. Moritani, "Novel insights into biarticular muscle actions gained from high-density electromyogram," *Exerc. Sport Sci. Rev.*, vol. 49, no. 3, pp. 179–187, 2021.